# Flow Control Experiments for Low Re Adaptive Airfoils

David E. Munday* & J. D. Jacob†
Department of Mechanical Engineering
University of Kentucky
Lexington, KY 40506-0108
E-mail: jdjacob@uky.edu

## Abstract

Effects of a an adaptive airfoil based on a flat-bottomed NACA 4415 are tested experimentally. Using a piezoelectric actuator to vary the profile of the airfoil, profile perturbations are predicted from which several rigid wing models were constructed. These are tested in a wind tunnel and tow tank to determine the change in wing efficiency due to variations in the profile at low Reynolds number. Three airfoils are tested from $Re = 5 \cdot 10^4$ to $Re = 5 \cdot 10^5$ at varying angles of attack. Preliminary comparisons are made with numerical predictions to demonstrate the effect of adaptive wing shaping on flight performance and the difficulty of predicting separated flow at low $Re$.

## INTRODUCTION

### The Flow Control Problem

The majority of flows of scientific interest or practical use are by nature turbulent and thus have both time dependency and non-linearity. This makes them generally unpredictable (though steady-state approximations can be made which may closely model the flow). The control of the flow field is then a non-trivial problem in all but the simplest of cases. Though flow control may be generally defined to be any method by which the behavior of the flow is modified, in this context we refer to the detailed manipulation of a flow field to achieve a desired change in some flow parameter, such as the control of separation or an increase in turbulent mixing. This can be either passive or active. It is the latter which is of more interest, since it has the ability to respond to changes in the flow field dynamically. However, it also requires the expenditure of energy and usually requires the flow to be monitored.

As a design tool, active flow control is not yet a mature technology, but the lure of its many practical uses makes it a much researched area of fluids engineering (e.g., Gad-el-Hak, 1996; Wygnanski, 1999). Much of the research in active flow control has focused on using surface blowing and/or suction or fluidic perturbation devices in an attempt to alter the boundary layer for modification of the larger flow field. Most recently, MEMS have offered some hope of practical flow control in the near future. In essence, current flow control devices in wall-bounded flows actively alter the flow field so that it adapts to the wall geometry. Since most flows are turbulent but the surfaces in the flow are designed using steady-state assumptions, some form of flow control can be used in almost every application. One may take the opposite approach, however, where the surface geometry actively adapts or morphs to changing flow conditions (e.g., Jacob, 1998). In essence, any fluidic device with moving parts such as a wing with control surfaces alters its effective geometry, though in a gross, inelegant and often inefficient manner. Ideally, one would like to change the actual geometry of the surface whereby the wall structures can change shape. This is more intuitive than the current flow control approach but more challenging to investigate and implement. It is this adaptive flow control concept that we are interested in here.[1]

### Adaptive Wings

To examine the possible practical uses of AFC, we shall recall one of its first implementations. The early days of aircraft saw extensive use of what we might today call AFC technology. The Wright brothers used

*Graduate student; member AIAA.
†Assistant Professor; senior member AIAA.



[1] In the remainder of this document, we shall refer to adaptive flow control as *AFC* and this should not be confused with active flow control. Adaptive flow control, by its very nature, is active.

wing warping, essentially twisting of the airfoil along its span, to control the wing's lift distribution, and hence the flight. This came from their analysis of bird flight, where they observed that birds controlled their motion by a "torsion of the tips of the wings." (Anderson, 1997) But aircraft called for wings capable of carrying more weight and this resulted in stronger and stiffer wings unable to warp. Since control surfaces offered performance comparable to or better than what the Wrights' developed, wing warping became obsolete. The benefits of bird-like, or pterygoidal, wings remain obvious though, since a wing capable of complex movement is more adaptable to a large range of flight conditions than the comparitively rigid structures we use as wings today. Attempts have been made over the years to make a wing variable, but truly adaptive wings capable of warping their geometry have remained unobtainable. Now however, wing warping in the true sense of the phrase is on the foreseeable horizon through the use of adaptive material technology. Adaptive wings, i.e., wings which vary geometric parameters in flight rather than passively interacting with the flow field, have been heavily researched in the last decade in the structures community (e.g., Austin *et al*, 1994; Hustedde *et al*, 1997). The promise of an adaptive wing is immense; an airfoil whose geometry is variable in flight can offer numerous advantages such as increased efficiency, higher stall angles through separation control, and greater maneuverability.

MEMS and other miniature devices have offered great promise in the field of active flow control in recent years, particularly for aerodynamic applications (Gad-el-Hak, 1994, 1996; Amitay *et al*, 1997; Kroo, 1999). MEMS can be used to control separation and hence enhance streamlining of a body. This is particularly true for bluff bodies, but the same can be said for lifting surfaces as well. Also, MEMS have the added benefit of acting as sensors as well as actuators so the flow can be actively altered with feedback control. Specifically, MEMS have been used as miniature flaps to reduce the amount of shear-stress on a wing (Ho and Tai, 1996). This has shown the promise of real-time turbulent shear stress control on a wing. However, MEMS are often complex systems with high manufacturing and maintenance costs. Expensive infrastructure is required for their development and the possibility of applying a large amount of MEMS technology to a flight vehicle in an inexpensive manner is uncertain. Most importantly, they rely on the philosophy that it is better to modify the flow to adapt to the geometry rather than modify the geometry to adapt to the flow.

The primary motive for altering wing geometry is to improve airfoil efficiency in off-design flight regimes. This concept is a standard implementation in most modern aircraft designs and takes the form of flaps which change the wing area and/or effective camber. A polymorph wing (variable planform) and variable pitch or incidence are also proven methods of wing adaptation. Adaptive concepts have taken many forms and names, including deformable, flexible, and active, in addition to those previously mentioned. In this paper, however, we will use the term *adaptive* to indicate an airfoil whose actual (as compared to effective) profile can be altered during flight.

The ideal use of an adaptive strategy allows the wing to vary its geometric parameters in flight during encounters with changing flow conditions such as wind speed or direction. As many of the governing principles of the unsteady fluid/structure interactions are unknown, extensive research into the physics is necessary, including the dynamics of series adaptive paneling, the actuation and control of an adaptive wing in flight, and real-time unsteady aerodynamic measurement and analysis. It is the dynamics of the fluid/structure interface that interest us here, primarily the aeroelastic transient coupling of the varying airfoil parameters and the unsteady flow. As the wing changes geometry, the flow will rapidly follow these changes. However, since the flow is a continually evolving structure, the altered flow field can interact with the wing in a nonlinear fashion. To determine the desired singular or periodic variations in wing geometry, it will be necessary to first understand the underlying physics. The number of variables result in an inordinately large parameter space which will require the use of simulations in tandem with any experimental investigation.

## Range of Interest

The qualitative aerodynamic characteristics of low $Re$ flows are typically vastly different than those normally seen in typical aerodynamic and aerospace applications [2, 3]. Slight changes in the flow speed can have large effects on the flow over a given airfoil, most notably large changes in L/D ratio. The wing shape can be specifically tailored for a certain $Re$, but designing for a larger range of $Re$ will degrade performance for a specific wing velocity. Two classes of aircraft fly in the low to moderate $Re$ range: Micro Aerial Vehicles ($\mu$AVs) and Unmanned Aerial Vehicles (UAVs or RPVs). In the former case, $Re$ may range from $10^4 - 10^5$ and lower if hovering/loitering vehicles are considered.

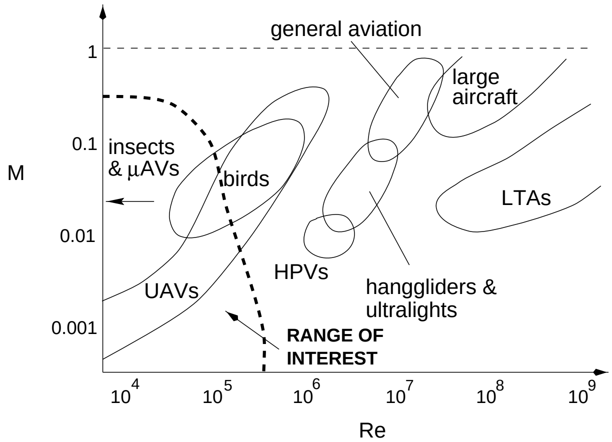


Figure 1: Range of interest on the Re-M diagram.

In the latter case, $Re$ typically increases from $10^5$ upwards to $10^6$ and higher for the larger faster aircraft. Due to the nature of these vehicles, the technology described herein is well suited for $\mu$AV and UAV application inasmuch as the Re range of these vehicles allows the flow to be easily adjusted using wing shaping [15].

Sub-scale air vehicles such as $\mu$AVs and UAVs often have the disadvantage of lower lift capabilities due to reduced size but increased weight penalties due to a minimum size of control surfaces. The primary advantage of a $\mu$AV is its small size allowing it to go unnoticed on the battlefield. It is ideally suited for covert operations where surprise and advanced intelligence are key components of a successful mission. The size limit of $\mu$AVs are typically given as less than 15 cm in maximum length [5, 15]. For a standard wing planform, this gives a span of $b = 15$ cm. If a moderate aspect ratio of 4 is assumed and the vehicle is to move at a relatively slow speed, say 10 m/s, an estimate for even high lift coefficients results in lift forces on the order of 0.5 N (0.1 lbs.) or less. This weight leaves little room for equipment, let alone the vehicle structure and powerplant itself. And if the vehicle were to encounter a gust in the same direction as flight, the vehicle would probably crash. Since $\mu$AVs are still in the early development stages, issues such as operation, safety, reliability, robustness, affordability, packaging and other operational factors cannot be adequately discussed.

As on option to $\mu$AV utilization, an adaptive wing can be installed on an UAV/RPV. This has many of the same characteristics of a $\mu$AV, only on a larger scale. UAVs are typically designed for a single mission in mind, usually long-range cruise. For UAVs which have varied mission goals, however, such as loiter, encounter, and then rapid return, the vehicle may experience a variety of flight regimes. An adaptive wing would be an ideal lifting system for such a vehicle. While it would be possible to retrofit an existing UAV with an adaptive wing, it would probably be more cost efficient to design a new UAV around an adaptive wing system.

### Adaptive Wing Developments

Conventional means of wing shaping require in-wing actuators and additional lifting surfaces. These are typically rigid attachments to the main wing and the profile is altered to an equivalent profile by gross adjustments. These are typically only good in a small range of $Re$ and $M$. To alter the wing profile in situ, internal actuators can be used to adjust such parameters as camber and thickness, but the adjustments are typically small and the actuators heavy. Thus, the benefits of wing shaping were outweighed by its added weight penalties.

One of the early departures from the philosophy which treated aircraft wings as rigid structures discussed the advantages of structural tailoring in aircraft [6]. This approach takes advantage of characteristics such as structural anisotropy and elastic coupling to enhance a particular structural response. This approach to airfoil design has been demonstrated to yield significant benefits. It provided the framework for subsequent investigations that added active elements to improve upon the already significant benefits of structural tailoring. Further studies examined in detail the interaction between aerodynamic forces, structural forces, conventional control forces, and an additional control force arising from inclusion of active materials in the wing structure [7]. A mathematical foundation was presented that argued that the inclusion of active materials in the wing structure could be used to advantage to increase wing speed divergence, reduce gust loading, and change lift effectiveness. It is clear that an ability to control these wing characteristics in a practical fashion would lead to a wing design which is beneficial to aircraft performance.

Active elements were added later to enhance structural tailoring effects [8]. This work was a largely experimental study where the static shape of a prototype F-14 wing cross-section was controlled with an array of linear actuators that acted as both wing spars and actuators to control wing shape. The stated goal of this study was the reduction of shock-induced drag in transonic cruise and multi-DOF shape control was demonstrated that could potentially address this problem.

Modeling of aeroelastic structural tailoring and adaptive wings (those that incorporate active materials) were more fully examined using a thick walled composite beam representative of the structure of a modern aircraft wing [9]. The wing model included anisotropy and coupling to allow structural tailoring and active layers to provide shape control. The results of this extensive modeling effort indicated that the combination of structural tailoring and adaptive wing shape control can improve the vibrational and static aeroelastic response of aircraft wings.

AFC using adaptive materials offers another solution to this problem. The most common of adaptive or smart material actuators are made of piezoelectric materials such as zinc oxide or lead zirconate titanate. These are based upon the piezoelectric effect where a force is generated by a piezoelectric material when a differential voltage is applied. These have to made relatively thick to prevent dielectric breakdown. Piezoelectric actuators can take many forms such as stacks or bimorphs. Both have been used with success in the construction of flaps for airfoils (Straub and Merkely, 1997) and helicopter blades (Clement *et al*, 1998). These can be used alone or in conjunction with traditional systems, such as hydraulic or mechanical actuators. Other smart materials used in aerodynamic applications include shape memory alloys (SMA) such as Nitinol. These are metals that change shape when the temperature of the material changes. This can be accomplished by electrical current heating or Joule heating and then allowing the system to cool whereby the material returns to its previous un-heated shape. This system is particularly suited for use in hydrofoils where cooling is rapid (Rediniotis *et al*, 1998).

The papers mentioned above represent an overview of the early work in adaptive wing modeling. This area has matured to the point where significant experimental verification work is now taking place. Recent tests of a piezoelectric actuator driven adaptive wing were used to demonstrate active flutter control [10]. Also discussed were tests investigating alleviation of vertical tail buffeting and wing shape control using piezoelectric actuators applied to load-bearing structural members. Development of wind tunnel models and results of wind tunnel tests of adaptive wing models have also been demonstrated [11, 12]. Both investigations lend credence to the basic concept of the adaptive wing as a practical design option for an aircraft wing. An adaptive airfoil design designated the Dynamically Deforming Leading Edge (DDLE) airfoil varies the leading edge radius in flight by stretching its thin composite skin [13]. The primary objective for this development is to achieve effective flow control over the airfoil through the reduction of strong adverse pressure gradient that leads to wing stall. Recent investigations into flexible wing architectures have shown the possibility of their use in adaptive wing technology as well [14, 15].

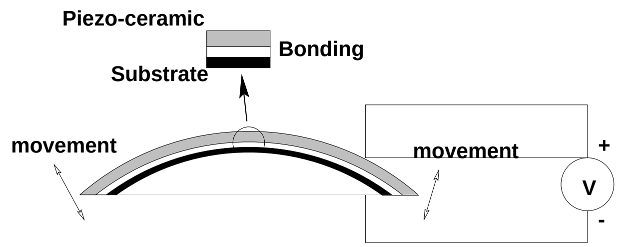


Figure 2: Piezoelectric THUNDER actuator.

A portion of an adaptive actuator using piezoelectric material. This specific design offers a good balance between force and deflection.

## Experimental Approach

The guiding philosophy of adaptive wing design is to find the most cost-efficient system using current or nearly available technology. Several guidelines must be considered when designing this subsystem. These include cost, weight, frequency response, force/deflection, and ease of control. Piezoelectric actuators offer a good balance between these systems. They also lend themselves well to novel applications. Such a design is shown in figure 2. A device such as this is currently under development for use in helicopter blades [17]. A piezoelectric material is bonded to a substrate. When a voltage is applied to the smart material, the actuator deflects. This deflection is easily controlled by the input voltage. In addition, this system can also be used as a sensor by measuring the output voltage for a given force/deflection input. Thus, this technology can be typically serve dual functions.

Experiments with a circular-arc airfoil suggest that an airfoil with oscillating camber will produce a higher lift coefficient than the same airfoil at any fixed camber setting [20]. The present experiment will attempt to extend this finding to airfoils of more ordinary and more efficient cross-section.

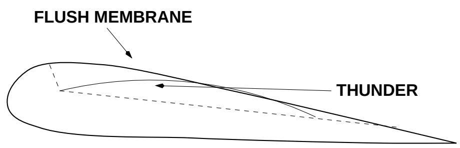


Figure 3: Adaptive wing using THUNDER – baseline.

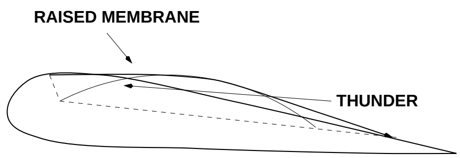


Figure 4: Adaptive wing using THUNDER – activated.

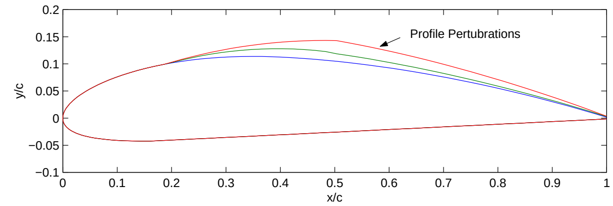


Figure 5: Wing profiles.

A modified NACA 4415 served as the baseline profile; perturbations due to simulated adaptation increased the maximum camber and moved its location aft.

## Test Articles

A molded airfoil section is to be constructed with a recess cut in the upper surface to receive the THUNDER actuator. The Thunder actuator is to be mounted in such a way that it is even with the un-recessed airfoil section when it is at its smallest effective radius. (When it is most curved). A thin fiberglass sheet will then be placed over the actuator to smooth the profile, an then the entire assembly will be wrapped in a latex membrane to hold it all together and provide a seamless outer surface. See figure 3.

When the THUNDER is at its smallest effective radius, the assembly will have the same cross-section as the base airfoil; and we would expect the flows and the coefficient of lift to be the same as the base airfoil. When the THUNDER is shifted to its greatest effective radius (closest to being flat) it will protrude through the upper cross-section. The fiberglass sheet and latex membrane will smooth the upper surface and the effective camber of the upper surface will be increased, furthermore the point of maximum thickness will be moved aft. This will increase the region of attached flow as shown in figure 4. A similar apparatus has been used in tests to reduce drag [21].

In the presently completed research, a series of five solid models matching the predicted profiles for the range of actuator settings were made. The models are identified by the effective radius of the actuator, which ranges from 4 to 8 inches. The profiles of foils 4, 6, and 8 are shown in figure 5. The base profile is a NACA 4415. The 4415 was chosen since it provided sufficient thickness to make room for the actuator and its attachment fittings, and because it is a relatively flat-bottomed foil. The profile was them modified slightly to make the bottom truely flat to ease surface finishing the models. The foils are eight inches in chord, and the modeled actuator has the leading edge of its active surface 1.1 inches behind, and .66 inches above the leading edge of the chord line. It is placed so that its tangent at the leading edge is 20 degrees above the chord angle. Solid models were then constructed for actuator radii of 4, 5, 6, 7, and 8 inches.

## Wind Tunnel

Measurements of lift and drag for three of the airfoils (4, 6, and 8) were made in a 12 inch by 12 inch wind tunnel. The model was mounted by its aft pressure surface on a sting as shown in figure 6. Splitter plates are used to minimize 3-D effects. Force measurements were taken over a range of angles of attack from -6 to +20 degrees, with measurements taken at one-degree intervals. Measurements were taken at Reynolds numbers of 250,000, 400,000 and 500,000. Corrections were made for blockage in accordance with Barlow, Rae and Pope [4]. Forces were measured by strain gages in the sting.

## Tow Tank

A miniature towing tank is used for the current experiments as shown in figure 7. The tank is approximately 4.0 m long and 0.38 m wide and deep. A traverse is pulled along the top of the carriage via two shafts extending the length of the tank. A syncrhomesh pulley system and timing belts are used to prevent slippage and allow maximum repeatability. A 1.6 kW (2 hp) motor drives the carriage system allowing the traverse

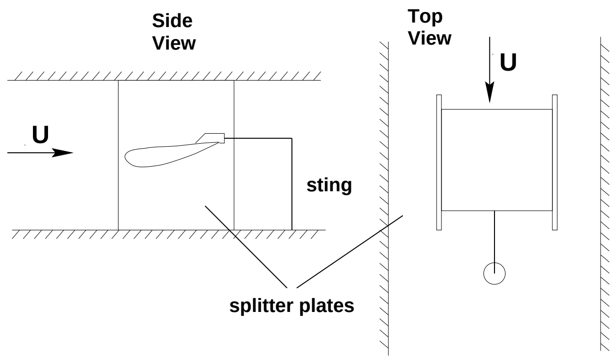


Figure 6: Wind tunnel setup.

The wing is mounted between two splitter plates.

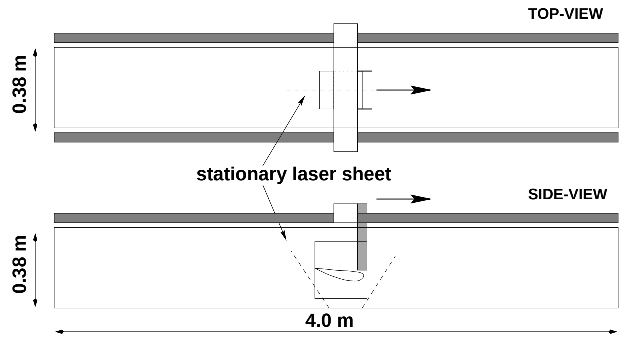


Figure 7: Tow Tank setup.

The wing is mounted between two end plates which are attached to the carriage.

to move up to 5 m/s. Models are suspended in the tank from the traverse with a 3 mm thick streamlined strut. The wing is mounted between two plexi-glass end plates which are connected to the struts.

A 5W Argon-Ion laser is used to create a laser sheet across the width of the tank. To measure spatial changes, or the evolution of the wake, the laser sheet is fixed relative to the laboratory reference frame, as shown in figure 7. To measure instantaneous temporal changes, the laser can be fixed relative to the airfoil by means of optics attached to the traverse. Silver-coated hollow glass spheres 10 $\mu$m in diameter are used as tracer particles. A Pulnix TM-6701 with a square-pixel CCD array (684×484 pixels) and a frame rate of 60/120 Hz is used to image the flow. Images are captured real-time to a PC using a Matrox Pulsar PCI frame grabber. LPT is used to extract the two-dimensional velocity and vorticity fields from the images as described below.

The Lagrangian parcel tracking (LPT) algorithm developed by Sholl and Savaş [22] is used to determine instantaneous flow fields from the tow tank experiments. The LPT algorithm regards seeding particles as fluid parcel markers and tracks both their translations and deformations. During this tracking, fluid parcels registered by individual CCD pixels are advected with individually estimated velocities and total accelerations. The velocity field needed to initialize the LPT process is obtained from a standard DPIV algorithm which uses multiple passes, integer window shifting, and adjustable windows. Both the LPT and DPIV algorithms employ a rigorous peak-detection scheme to determine velocity vectors and use the local velocity gradient tensor to identify spurious velocity vectors. We have found that the LPT algorithm works well in the flow field of a vortex which is characterized by high deformation rates where DPIV algorithms are plagued by biasing and limited dynamic range. No smoothing algorithms or other post-processing techniques are employed on the data. In the tow tank data, vorticity, being a component of the velocity gradient tensor, is calculated spectrally at each grid point as an intrinsic part of the LPT algorithm.

## Preliminary Results

### Wind Tunnel

243 runs were made in the wind tunnel at $Re = 250,000$, $400,000$, and $500,000$. Angle of attack was varied from -6 to +20 in 1 degree increments. $C_l$ and $C_d$ were recorded for each run. Plots of the measured results (figures 8, 10 and 12) show a clear change in the rate of change of lift with alpha at the stall. For the less perturbed airfoils (foils 4 and 6) the lift coefficient levels or falls off above stall, but the most perturbed foil (foil 8) shows a continuing increase in lift with increase in alpha above stall angle.

### Tow Tank

75 runs were made in the tow tank with 5 separate airfoils (wings 4, 5, 6, 7, and 8). Carriage speed was varied to acheive $Re$ of $5 \cdot 10^4$, $1 \cdot 10^5$, $2.5 \cdot 10^5$, $4 \cdot 10^5$ and $5 \cdot 10^5$ at angles of attack of 2.3°, 8.3°, and 14.3°. A single pair of images was processed for each run as discussed above resulting in a single velocity field in the laboratory's frame of reference. Conversion to

| Figure | Wing | $\alpha$ | $Re$ |
|---|---|---|---|
| 14 | 4 | 2.3° | $5 \cdot 10^4$ |
| 15 | | | $1 \cdot 10^5$ |
| 16 | | | $2.5 \cdot 10^5$ |
| 17 | 6 | 2.3° | $5 \cdot 10^4$ |
| 18 | | | $1 \cdot 10^5$ |
| 19 | | | $2.5 \cdot 10^5$ |
| 20 | | | $4 \cdot 10^5$ |
| 21 | 8 | 2.3° | $5 \cdot 10^4$ |
| 22 | | | $1 \cdot 10^5$ |
| 23 | | | $2.5 \cdot 10^5$ |
| 24 | | | $4 \cdot 10^5$ |

the wing's frame of reference is acheived by subtracting the wing's velocity from the velocity field. Only the attack angles of 2.3° are presented in this paper for 3 wings (numbers 4, 6, and 8). Parameters are shown in table while vector plots are given in figures 14 to 24, respectively.

Separation is clearly seen at the lowest $Re$ for all 3 wings. As expected, separation decreases as $Re$ increases These vector plots will be used to determine the points of separation and the velocity profiles over the surface. Shear stress comparisons will be made to determine the skin friction coefficient for use in determining incipient separation parameters. Data is currently being reduced for for the remaining 64 experimental runs.

### Comparison with Predictions

As a test of the capability of predictive tools, comparisons of the experimental results are made with Xfoil [23]. The results are depicted in figures 9, 11 and 13.

The graphs illustrate two points. (1) Slight variations in geometry (here, an approximate increase of 3% in maximum thickness) can have a large impact in the aerodynamic performance. (2) More importantly, prediction of aerodynamic parameters at low $Re$ is problematic at best, requiring experiments that examine the performance of airfoils in this $Re$ range.

## Summary

Effects adaptation of modified NACA 4415 were tested experimentally. These adaptations model use of a piezoelectric actuator to vary the profile of the airfoil. The model airfoils were tested in a wind tunnel and tow tank to determine the change in wing efficiency due to variations in the profile at low Reynolds number. 3 airfoils were tested from $Re = 5 \cdot 10^4$ to $Re = 5 \cdot 10^5$ at varying angles of attack.

Comparison of the results of these tests show difficulty in reliance on numerical predictions from a product such as Xfoil.

Future work will construct an airfoil with piezoelectric actuation, and examine its behavior both at fixed camber settings and with an oscilating camber.

# References

[1] J. D. Jacob. On the fluid dynamics of adaptive airfoils. Proc. of the 1998 ASME International Mechanical Engineering Congress and Exposition, Anaheim, CA, 1998.

[2] Lissaman, P. B. S., "Low-Reynolds-Number Airfoils," *Annual Review of Fluid Mechanics*, **15**, 223-39, 1983.

[3] Mueller (ed.), T. J. *Low Reynolds Number Aerodynamics*, Springer-Verlag, New York, 1989.

[4] Barlow, B. B., Rae, W. H., Jr. and Pope, A. *Low-Speed Wind Tunnel Testing*, John Wiley & Sons, New York, 1999.

[5] McMichael, J. M. and Francis, M. S., "Micro Air Vehicles - Toward a New Dimension in Flight," DARPA Document, 1997.

[6] Weisshaar, T.A., "Aeroelastic Tailoring-Creative Use of Unusual Materials," AIAA Paper 87-0976, April 1987.

[7] Ehlers, S.M., and Weisshaar, T.A., "Static Aeroelastic Behavior of an Adaptive Laminated Piezoelectric Composite Wing," AIAA Paper 90-1078-CP.

[8] Austin, J., Rossi, M.J., Van Nostrand, W., G. Knowles, G., and Jameson, A., "Static Shape Control for Adaptive Wings," *AIAA Journal*, V. 32, No. 9 (September 1994), pp. 1895-1901.

[9] Librescu, L. Meirovitch, L. and Song, O., "Integrated Structural Tailoring and Control Using Adaptive Materials for Advanced Aircraft Wings, " *Journal of Aircraft*, Vol. 33, No. 1 (January-February 1996), pp. 203-213.

[10] Pinkerton, J. L., McGowan, A.R., Moses, R.W., Scott, R.C. and Heeg, J., "Controlled Aeroelastic Response and Airfoil Shaping Using Adaptive Materials and Integrated Systems," SPIE Paper 0-8194-2092-1 in SPIE Vol. 2717, pp. 166-177, 1994.

[11] Hustedde, C. L., S. F. McGrath, M. A. Hopkins, K.E. Griffin, "Further Investigations of the Aeroelastic Tailoring for Smart Structures Concept," Proceedings of the AIAA 38th Structures and Structural Dynamics Conference, Kissimmee, Florida, April 7-10, 1997, AIAA Paper 97- 1164.

[12] Kudva, J., Appa, K., Martin, C. A., Jardine, A. P., Sendeckyj, G., Harris, T., McGowan, A., and Lake, R., "Design, Fabrication, and Testing of the DARPA / Wright Lab Smart Wing Wind Tunnel Model," Proceedings of the AIAA 38th Structures and Structural Dynamics Conference, Kissimmee, Florida, April 7-10, 1997, AIAA Paper 97-1198.

[13] Chandrasekhaara, M.S., Wilder, M. C., and Carr, L. W., "Design and development of a Dynamically Deforming Leading Edge Airfoil for Unsteady Flow Control," *ICIASF '97*, 1997.

[14] Kim, S.-H. and Lee, I., "Aeroelastic Analysis of a Flexible Airfoil with a Freeplay Non-linearity," *Journal of Sound and Vibration*, 193(4):823–846, 1996.

[15] Shyy, W. and Smith, R., "A Study of Flexible Airfoil Aerodynamics with Application to Micro Aerial Vehicles," AIAA 97-1933, *28th AIAA Fluid Dynamics Conference*, June, 1997.

[16] Straub, F. K. and Merkley, D. J. , "Design of a smart material actuator for rotor control," *Smart Materials and Structures*, 6:26-34, 1997.

[17] Clement, J. W., Brei, D., Moskalik, A. J., and Barrett, R., "Bench-top Characterization of an Active Rotor Blade Flap System Incorporating C-Block Actuators," 39th AIAA/ASME/ASCE/AHS/ASC Structures, Structural Dynamics, and Materials Conference and Exhibit, AIAA-98-2108, 1998.

[18] Rediniotis, O. K., Lagoudas, D. C., Garner, L. J., and Wilson, N., "Experiments and Analysis of an Active Hydrofoil with SMA Actuators," AIAA 36th Aerospace Sciences Meeting and Exhibit, AIAA-98-0102, 1998.

[19] H. S. Tzou. "Development of a light-weight robot end-effector using polymeric piezoelectric bimorhp," *Proc. of the 1989 IEEE International Conference on Robotics and Automation*, Scottsdale, AZ, 1989.

[20] N. J. Pern. "Vortex Mitigation Using Adaptive Airoils." M. S. Thesis, University of Kentucky, 1999.

[21] T. L. Pinkerton and R. W. Moses, "A Feasibility Study to Control Airfoil Shape Using THUNDER," NASA TM 4767, 1997.

[22] M. J. Sholl and Ö Savaş. A fast Lagrangian PIV method for study of general high-gradient flows. In *AIAA 35th Aerospace Meetings & Exhibits*. AIAA, 1997. Paper 97-0493.

[23] M. Dreka, "XFOIL: An Analysis and Design System for Low Reynolds Number Airfoils," *Low Reynolds Number Aerodynamics*, Springer-Verlag, 1993.

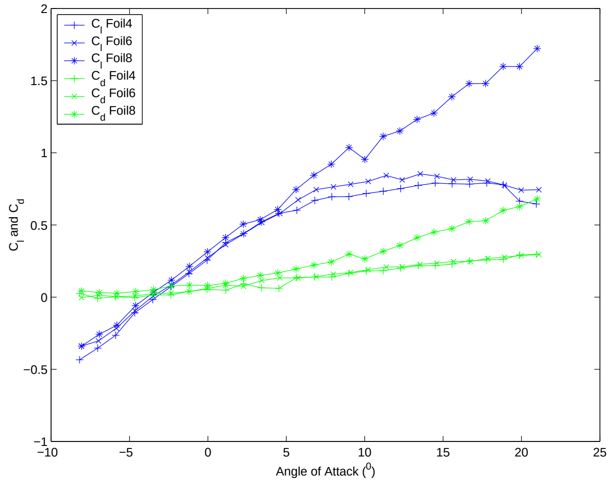


Figure 8: Wind tunnel data. Re=250,000.

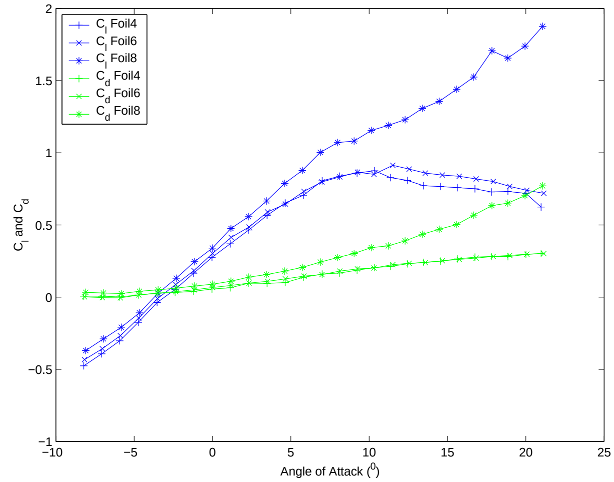


Figure 10: Wind tunnel data. Re=400,000.

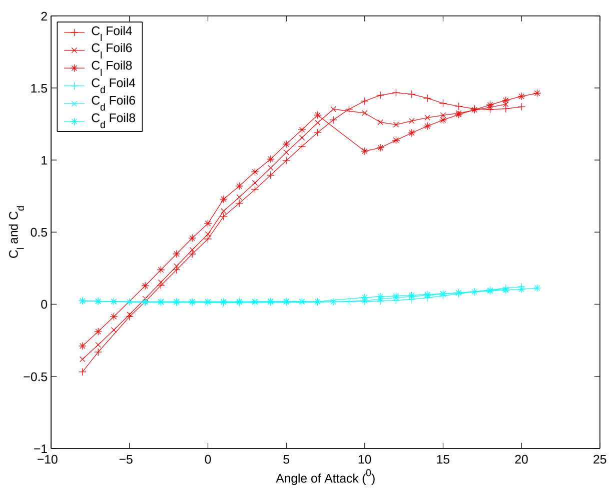


Figure 9: Xfoil predictions. Re=250,000.

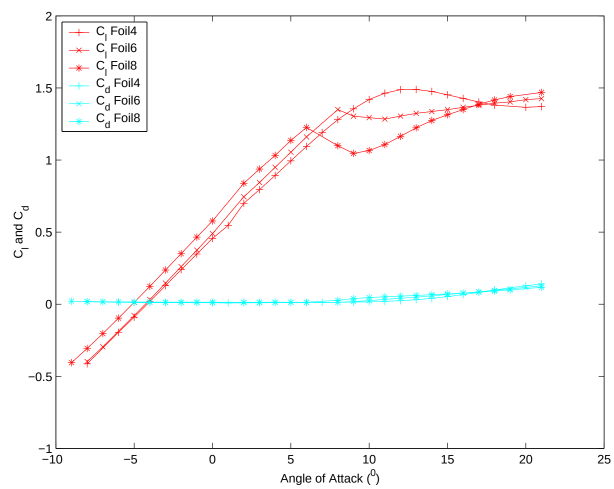


Figure 11: Xfoil predictions. Re=400,000.

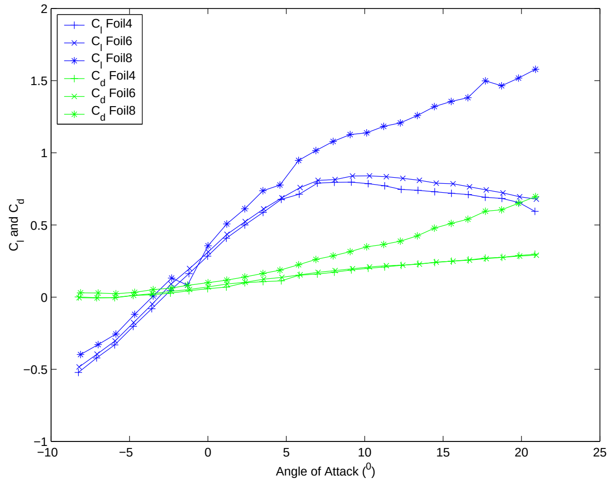


Figure 12: Wind tunnel data. Re=500,000.

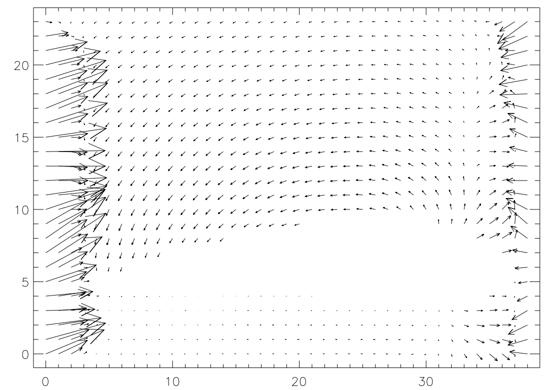

Figure 14: Wing 4, $Re = 5 \cdot 10^4$,$\alpha = 0^o$.

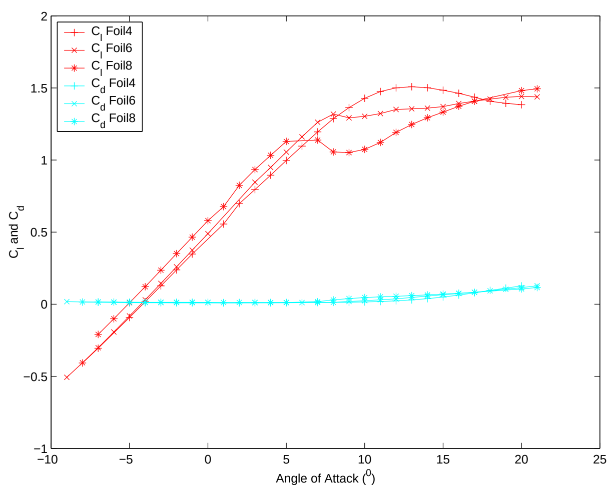


Figure 13: Xfoil predictions. Re=500,000

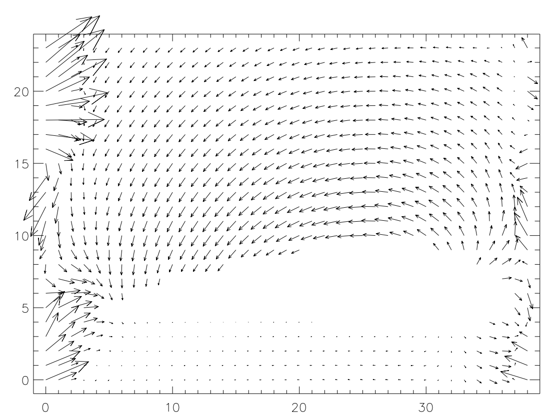

Figure 15: Wing 4, $Re = 1 \cdot 10^5$,$\alpha = 0^o$.

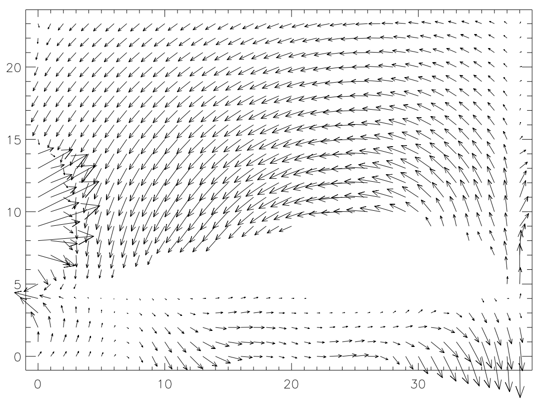


Figure 16: Wing 4, $Re = 2.5 \cdot 10^5$,$\alpha = 0^o$.

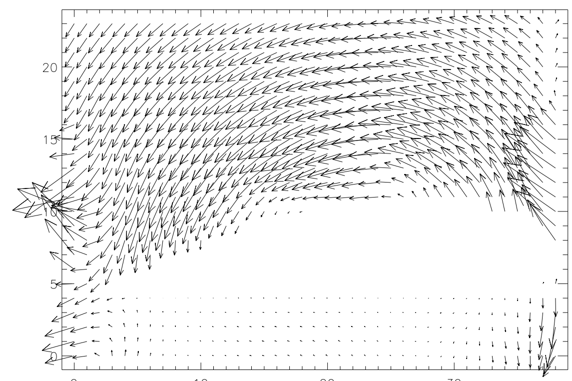


Figure 18: Wing 6, $Re = 1 \cdot 10^5$,$\alpha = 0^o$.

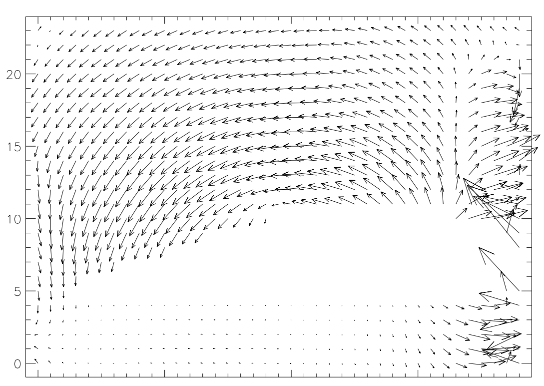


Figure 17: Wing 6, $Re = 5 \cdot 10^4$,$\alpha = 0^o$.

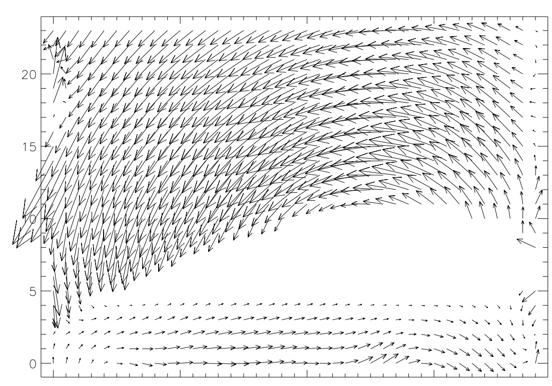


Figure 19: Profile 6, $Re = 2.5 \cdot 10^5$,$\alpha = 0^o$.

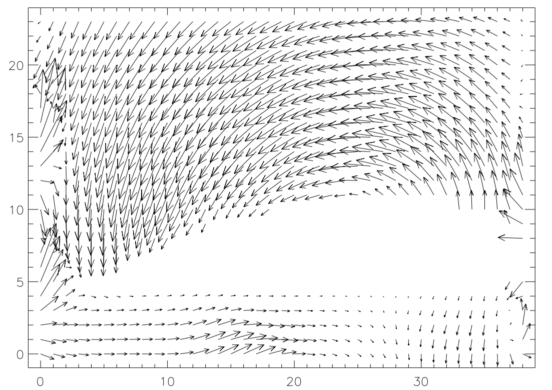

Figure 20: Wing 6, $Re = 4 \cdot 10^5$,$\alpha = 0^o$.

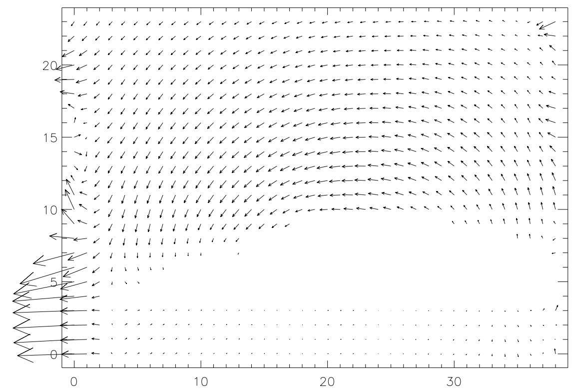

Figure 22: Wing 8, $Re = 1 \cdot 10^5$,$\alpha = 0^o$.

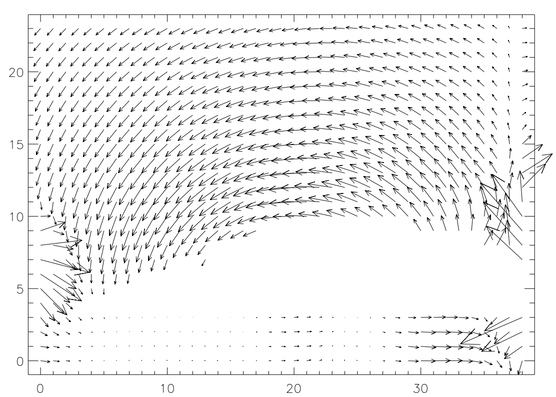

Figure 21: Wing 8, $Re = 5 \cdot 10^4$,$\alpha = 0^o$.

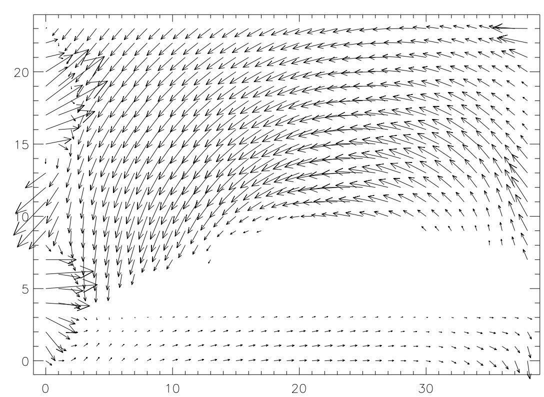

Figure 23: Wing 8, $Re = 2.5 \cdot 10^5$,$\alpha = 0^o$.

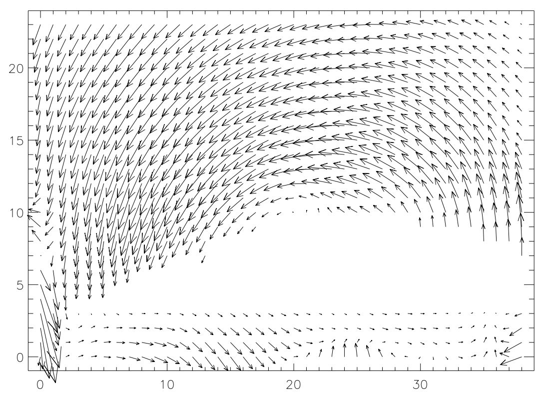


Figure 24: Wing 8, $Re = 4 \cdot 10^5$,$\alpha = 0^o$.